Chapter 2: Multimode Theory of Gyrotron Oscillators

2.1 Introduction

In the preceding chapter, the background and classification of microwave tubes were discussed. The drift of the electron beam produces free energy through a diffuse medium that can be used to produce electromagnetic waves in the RF interaction structure. Initially, the research interest was focused on the interaction of slow-space charged waves with the propagation of electron beams in the medium [80]. Later on, gyro-devices have been developed that gave better results than the conventional devices and replaced the conventional devices in terms of generating continuous-power radiation at millimeter-wave, submillimeter-wave and THz regime.

Instability in a beam-wave coupled system can be understood with interactions between slow or fast space charge waves and electromagnetic waves in waveguide structures. The waves with phase velocity slower than electron beam velocity in the propagation direction are called slow-wave devices. On the other hand, fast space charged waves are referred to as fast-wave devices with faster phase velocities than electron beam velocities. Among the many configurations of gyro-devices, the gyro-monotron, commonly known as the gyrotron oscillator, employs a periodic coupling electron beam in a smooth-wall interaction structure that supports a fast waveguide mode. The interaction mechanism of gyrotrons is based on electron cyclotron resonance measure (ECRM) instability and can be operated at higher harmonics of the waveguide and beam cyclotron harmonic modes than slow-wave devices and allows for larger transverse amplitudes of the interaction structure. This leads to the generation of high output power using practical values in the applied DC magnetic field. Theoretical descriptions of CRM instability [81] were described in chapter – 1. A gyrotron oscillator can deliver few watts to MW in pulse and CW of output power from millimeter-wave to THz regime. A review of low power gyrotrons has been presented in

the past by several authors [40, [47], [82]. High-frequency gyrotron researches have steadily improved over the past two decades. Some high-frequency gyrotron experiments have been described in various kinds of literature [30], [83] – [84].

Various approaches to the design and analysis of gyrotrons have been reported in much independent research works in the literature [9], [85] – [87]. To demonstrate and investigate the RF beam-wave interaction behavior of gyrotrons, linear and non-linear theories have been developed as given in [1], [9], [88] – [94]. In linear theory, the electron beam is characterized by a distribution function that corresponds to a density function and depends on space, time, and speed. The beam's velocity and guiding center spread can also be implemented to it, but its arithmetic becomes very complex. The relativistic Vlasov equation is used to obtain the perturbed electron distribution function in the presence of electromagnetic waves [7]. These perturbations are linearized to obtain analytical values. Linear theory can predict start oscillation conditions and dispersion relation, which can provide guidelines for the design of a stable device.

On the other hand, a nonlinear theory is used to predict the output power, efficiency, and bunching phenomena of electrons thereby allowing the saturation mechanism to be better understood. Nonlinear analysis can include the drift of the electron guiding center, the effect of spreading velocity, and impurities of the applied magnetic field and any form of interaction structure. Another advantage of this method is that the saturation effect can also be taken into account due to electron overtaking and electron bunch deflection from the RF phase, resulting in a better explanation for nonlinearity. In several published research works [88] – [91], Multimode ideas have been presented using nonlinear theory.

At high frequency, the cavity's transverse dimension is reduced, causing gyrotron to operate at higher-order modes by using an oversized interaction structure

that invokes mode compaction in the cavity. Higher magnetic fields are required at higher frequencies that cause the device to operate on harmonics that afflict mode competition from nearby modes as well as fundamental modes [95] – [96]. Due to the high density of the mode spectrum in the cavity, the device switches to the parasitic mode which affects the device's efficiency. The correct power and efficiency of the device can be estimated using the Multimode principle, which incorporates all nearby modes inside the cavity. In the Multimode theory, competing modes' effect is studied using a fully nonlinear formulation done by Fliflet *et al*. [91].

In the present chapter, the gyrotron's analysis and design are presented to study the beam-wave interaction behavior of the cavity. The analysis is reviewed here to observe the features that are required for gyrotron oscillator design. Generalized nonlinear theories involving the presence of Multimode are presented to study the beam-wave interaction mechanism. These analyses also include the second-harmonic operation of the device. The electron dynamic equations are represented as phases and momentum, resulting in simplifying the equations and substantially reducing the number of equations. In this approach, the waveguide's excitation equation is initially determined in the absence of the beam, and then the effect of the beam on the RF cavity field profile is observed. Then, it is possible to calculate the output power and efficiency according to the set of beam parameters. In this analysis, the effects of electron beam spread, the drift of guiding and non-uniform DC magnetic field conditions can also be taken into account.

The self-consistent time-dependent Multimode theory is briefly described in section 2.2. The design methodology and the limiting constraints of the gyrotron cavity

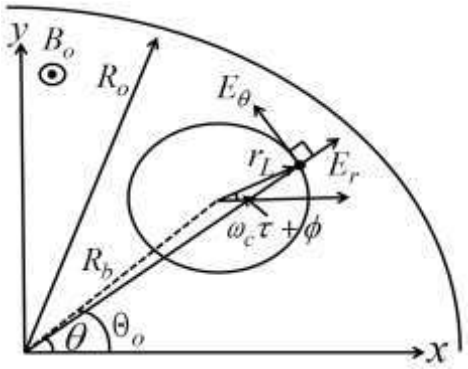

Figure 2.1 The arrangement of electrons in the Larmor orbit with cylindrical coordinates and Cartesian coordinates.

are discussed in section 2.3. Furthermore, the results obtained from the Multimode analysis are discussed in section 2.4. Finally, the chapter is concluded in section 2.5.

2.2 Multimode Theory

In single mode theory, a single-mode excitation is considered in the gyrotron cavity. However, in overmoded cavities, the mode spectrum is very dense, so it is difficult to avoid mode competition in cavities that destabilize the gyrotrons operation and reduce its efficiency. Therefore, a self-consistent Multimode theory is described based on the formulation by Fliflet *et al.* [91], in which the performance of the gyrotron cavity is observed in the presence of several modes in the overmoded cavities. In self-consistent calculations, the equations of motion for the electrons are solved simultaneously with the field equations, taking into account the beam's effect on the cavity field profile and quality factor of the cavity [1].

In this analysis, a thin annular electron beam is considered. The electron beam arrangement in a cylindrical cavity with all the coordinates is shown in Figure 2.1. The electrons follow a helical path around the center guiding radius R_b. It is assumed that the electron beam interacts with one or more competing modes in the cavity. To govern the

motion of electrons in the presence of a perturbing RF field, Lorentz's force equation is given as,

$$\frac{dP}{dt}+\frac{|e|}{\gamma m_e}P\times B_o=|e|\left(E+\frac{1}{\gamma m_e}P\times B\right)\equiv a' \tag{2.1}$$

where, P is the momentum of the electron, B_o is the applied magnetic field $\left(B_o=B_o\hat{z}\right)$. E and B are the electric field and magnetic field, m_e is the rest mass of an electron, and γ is the relativistic factor given as $\gamma=\left[1+P^2/\left(m_e c\right)^2\right]^2$.

The interaction of electrons with RF fields causes perturbations in their momentum and phase, i.e. their momentum and phase deviate from normal values that they would not have interacted with. The Cylindrical-coordinate system is considered in this context to facilitate changes in the momentum and phase of electrons and with an overview of the most appropriate coordinate system. So, the transverse momentum of the electron can be written as,

$$p_x+ip_y=ip_t\exp\left[i\left(\omega_c\tau+\phi\right)\right] \tag{2.2}$$

where, p_t and ϕ are the magnitude and phase of transverse momentum on a slow time scale, respectively. The term slow time scale indicates that those temporal derivatives of momentum and phase are slightly lower than the operating frequency (ω_o) or reference cyclotron frequency (ω_c). Before considered the interaction between beam and wave, the above equation (2.2) can be written as,

$$p_x+ip_y=ip_t\exp\left[i\left(\omega_c\tau+\phi_o\right)\right] \tag{2.3}$$

where, ϕ_o is the initial gyro-phase of the electron beam in the beamlets and p_t is given as $\left[p_x^2+p_y^2\right]^{1/2}$. After doing some mathematical manipulation in equation (2.1) can be rewritten as,

$$a'_x + ia'_y = \frac{dp_x}{dt} + i\frac{dp_y}{dt} + \frac{\gamma_o}{\gamma}\omega_c\left(p_y - ip_x\right) \tag{2.4}$$

$$a'_x - ia'_y = \frac{dp_x}{dt} - i\frac{dp_y}{dt} + \frac{\gamma_o}{\gamma}\omega_c\left(p_y + ip_x\right) \tag{2.5}$$

After differentiating the equation (2.2) with respect to t and taking complex conjugate, it is written as,

$$\frac{dp_x}{dt} + i\frac{dp_y}{dt} = ip_t \exp\left[i\left(\omega_c\tau + \phi\right)\right]\left(i\omega_c + i\frac{d\phi}{dt}\right) + i\exp\left[i\left(\omega_c\tau + \phi\right)\right]\frac{dp_t}{dt}$$

$$ip_x - p_y = -p_t \exp\left[i\left(\omega_c\tau + \phi\right)\right]$$

By substituting the above expression in equation (2.4) and (2.5), it is obtained as,

$$\left[a'_x + ia'_y\right]\exp\left[-i\left(\omega_c\tau + \phi\right)\right] = -p_t\left(\omega_c\tau + \frac{d\phi}{dt}\right) + i\frac{dp_t}{dt} + \frac{\gamma_o}{\gamma}\omega_c p_t \tag{2.6}$$

$$\left[a'_x - ia'_y\right]\exp\left[i\left(\omega_c\tau + \phi\right)\right] = -p_t\left(\omega_c\tau + \frac{d\phi}{dt}\right) - i\frac{dp_t}{dt} + \frac{\gamma_o}{\gamma}\omega_c p_t \tag{2.7}$$

Further, by addition and subtraction of the above equation, it is obtained as,

$$\frac{dp_t}{dt} = \frac{i}{2}\left\{\left(a'_x - ia'_y\right)\exp\left[i\left(\omega_c\tau + \phi\right)\right] - \left(a'_x + ia'_y\right)\exp\left[-i\left(\omega_c\tau + \phi\right)\right]\right\} \tag{2.8}$$

$$\frac{d\phi}{dt} = -\frac{1}{2}\left\{\left(a'_x - ia'_y\right)\exp\left[i\left(\omega_c\tau + \phi\right)\right] + \left(a'_x + ia'_y\right)\exp\left[-i\left(\omega_c\tau + \phi\right)\right]\right\} \times \frac{1}{p_t} - \omega_c\left(1 - \frac{\gamma_o}{\gamma}\right) \tag{2.9}$$

and the derivative of p_z is defined as

$$\frac{dp_z}{dt} = a'_z \tag{2.10}$$

The transverse component of the electric field and magnetic field for *TE* mode in the waveguide can be written as,

$$E_t = \mathrm{Re}\left\{\sum_{n=1}^{N} A_n\left(z,t\right)e_n\left(r,\theta\right)e^{-i\omega_o t}\right\} \tag{2.11}$$

$$B_t = \mathrm{Re}\left\{\sum_{n=1}^{N} -\frac{i}{\omega_o}\frac{\partial}{\partial z} A_n(z,t) b_n(r,\theta) e^{-i\omega_o t}\right\} \tag{2.12}$$

where, $e_n = \hat{z} \times \nabla_t \psi_n$ and $b_n = -\nabla_t \psi_n$ are the vector functions. ψ_n is the scalar or membrane function of n[th] mode that satisfies the Helmholtz equation. A_n (z, t) is the field amplitude. N is the number of modes that are considered to interact with the RF wave in the cavity. The axial components are given by,

$$B_z = \mathrm{Re}\left\{\sum_{n=1}^{N} \frac{ik_t^2}{\omega_o} A_n(z,t) \psi_n e^{-i\omega_o t}\right\} \tag{2.13}$$

The membrane function ψ_n is given by,

$$\psi_n(r,\theta) = C_{m_n l_n} J_{m_n}\left(k_{m_n l_n} r\right) \exp\left[i m_n \theta\right] \tag{2.14}$$

and, $C_{m_n l_n}$ is known as the TE mode normalization coefficient of the RF wave to the electron beam,

$$C_{m_n l_n} = \left\{\sqrt{\pi\left(\chi_{m_n l_n}^2 - m^2\right)} * J_{m_n}\left(\chi_{m_n l_n}\right)\right\}^{-1} \tag{2.15}$$

After defining the RF fields, the components a_x', a_y' and a_z' can be obtained subsequently. By using the conversion from Cartesian coordinates to cylindrical coordinates, the momentum vector P in the equation (2.1) can be written as,

$$P = p_t \cos(\varphi - \theta)\hat{r} + p_t \sin(\varphi - \theta)\hat{\theta} + p_z \hat{z} \tag{2.16}$$

where, $\varphi = \omega_c \tau + \phi$. In equation (2.11) and (2.12), the term b_n and e_n are expressed in cylindrical coordinates as, $e_n = \hat{z} \times \nabla_t \psi_n = -\frac{1}{r}\frac{\partial \psi}{\partial \theta}\hat{r} + \frac{\partial \psi}{\partial r}\hat{\theta}$, and $b_n = -\nabla_t \psi_n = -\frac{\partial \psi}{\partial r}\hat{r} - \frac{1}{r}\frac{\partial \psi}{\partial \theta}\hat{\theta}$, therefore the electric field and magnetic field are obtained as,

$$E_r = \mathrm{Re}\left\{\sum_{n=1}^{N} -C_{m_n l_n}\frac{im_n}{r}A_n(z,t)J_{m_n}\left(k_{m_n l_n}r\right)\exp\left[i\left(m_n\theta-\omega_o t\right)\right]\right\}$$

$$E_\theta = \mathrm{Re}\left\{\sum_{n=1}^{N} C_{m_n l_n}k_{m_n l_n}A_n(z,t)J'_{m_n}\left(k_{m_n l_n}r\right)\exp\left[i\left(m_n\theta-\omega_o t\right)\right]\right\}$$

$$B_r = \mathrm{Re}\left\{\sum_{n=1}^{N} C_{m_n l_n}\frac{i}{\omega_o}\frac{\partial}{\partial z}A_n(z,t)k_{m_n l_n}J'_{m_n}\left(k_{m_n l_n}r\right)\exp\left[i\left(m_n\theta-\omega_o t\right)\right]\right\}$$

$$B_\theta = \mathrm{Re}\left\{\sum_{n=1}^{N} C_{m_n l_n}\frac{-1}{\omega_o}\frac{\partial}{\partial z}A_n(z,t)\frac{m_n}{r}J_{m_n}\left(k_{m_n l_n}r\right)\exp\left[i\left(m_n\theta-\omega_o t\right)\right]\right\}$$

$$B_z = \mathrm{Re}\left\{\sum_{n=1}^{N} C_{m_n l_n}\frac{i}{\omega_o}A_n(z,t)k_t^2 J_{m_n}\left(k_{m_n l_n}r\right)\exp\left[i\left(m_n\theta-\omega_o t\right)\right]\right\}$$

Now, $P\times B$ can be written as

$$P\times B = \left[p_t\sin\left(\varphi-\theta\right)B_z - p_z B_\theta\right]\hat{r} - \begin{bmatrix} p_t\cos\left(\varphi-\theta\right)B_z \\ -p_z B_r \end{bmatrix}\hat{\theta} + \left[p_t\cos\left(\varphi-\theta\right)B_\theta - p_t\sin\left(\varphi-\theta\right)B_r\right]\hat{z} \qquad (2.17)$$

Therefore,

$$a'_r = -|e|\left(E_r + v_t\sin\left(\varphi-\theta\right) - v_z B_\theta\right)$$

$$a'_\theta = -|e|\left(E_\theta + v_t\cos\left(\varphi-\theta\right) + v_z B_r\right)$$

$$a'_z = -|e|\left(v_t\cos\left(\varphi-\theta\right)B_\theta - v_z\sin\left(\varphi-\theta\right)B_r\right)$$

After taking the simplest expression of a'_z from the above and some mathematical manipulations, the following expression are obtained as,

$$a'_z = -|e|v_t\,\mathrm{Re}\left\{\begin{array}{l}\sum_{n=1}^{N}\frac{C_{m_n l_n}k_{m_n l_n}}{\omega_o}\frac{\partial}{\partial z}A_n(z,t)\left[J_{m_n-1}\left(k_{m_n l_n}r\right)\exp\left[i\left(m_n-1\right)\theta-\omega_o t+i\varphi\right]\right]+ \\ J_{m_n+1}\left(k_{m_n l_n}r\right)\exp\left[i\left(m_n+1\right)\theta-\omega_o t-i\varphi\right]\end{array}\right\} \qquad (2.18)$$

Considering the beam's finite radius, the interaction of the RF wave with the electron beam should be considered by taking the coordinate system centered at the center of the beamlets, rather than the coordinate system centered along the axis of the cavity. The transformation of this coordinate system is performed using Graf's addition theorem [25]. It is a special general case of Newman's addition theorem, which can be expressed in the following form,

$$C_v\left(\eta r_j\right)\exp\left[iv\left(\theta_j-\vartheta_{jl}\right)\right]=\sum_{\mu=-\infty}^{\infty}C_{v+\mu}\left(\eta R_{jl}\right)J_\mu\left(\eta r_l\right)\exp\left[i\mu\left(\pi-\theta_l+\vartheta_{jl}\right)\right]\quad j\neq l \tag{2.19}$$

where, C_v can represent any of the Bessel functions J_v, I_v, Y_v, K_v, $H_v^{(1)}$, and $H_v^{(2)}$. (r_v, θ_v) and (r_l, θ_l) are polar coordinates centered at two different positions with global coordinates O_j, O_l. (R_{jl}, φ_{jl}) are the polar coordinates of O_l with respect to O_j. This expression is valid only provided that $r < R_{jl}$ (although this restriction is unnecessary if $C = J$ and v is an integer). The right-hand side of the equation (2.19) can be written in a suitable form to apply the Graf's theorem as,

$$a_z'=|e|\nu_t\,\mathrm{Re}\left\{\sum_{n=1}^{N}\frac{C_{m_nl_n}}{\omega_o}\frac{\partial}{\partial z}A_n\left(z,t\right)e^{-i\omega_o t}\left[\begin{matrix}e^{i(m_n-1)\theta_o+i\varphi}J_{m_n-1}\left(k_{m_nl_n}r\right)\exp\left[i\left(m_n-1\right)\left(\theta-\theta_o\right)\right]\\+e^{i(m_n+1)\theta_o-i\varphi}J_{m_n+1}\left(k_{m_nl_n}r\right)\exp\left[i\left(m_n+1\right)\left(\theta-\theta_o\right)\right]\end{matrix}\right]\right\} \tag{2.20}$$

After the transformation in the new coordinate system using the above theorem, the following changes occur in the right-hand side of the above equation (2.20),

$$\sum_{\mu=-\infty}^{\infty}J_{m_n-\mu}\left(k_{m_nl_n}R_o\right)J_{-\mu+1}\left(k_{m_nl_n}r_L\right)e^{-i(\mu-1)\left(\frac{\pi}{2}-\varphi+\theta_o\right)},\ \text{and}$$

$$\sum_{\mu=-\infty}^{\infty}J_{m_n+1-\mu}\left(k_{m_nl_n}R_o\right)J_{-\mu-1}\left(k_{m_nl_n}r_L\right)e^{-i(\mu+1)\left(\frac{\pi}{2}-\varphi+\theta_o\right)},\ \text{respectively.}$$

By applying a single harmonic condition $(\mu=s)$, where s is a harmonic number and replacing φ by $\omega_c\tau+\phi$, which can be expressed as,

$$\frac{dp_z}{dt}=a_z'=|e|\nu_t\,\mathrm{Re}\left\{\sum_{n=1}^{N}\frac{C_{m_nl_n}}{\omega_o}\frac{\partial}{\partial z}A_n\left(z,t\right)\left[\left(-i\right)^{s-1}J_{m_n-s}\left(k_{m_nl_n}r_b\right)\frac{\partial J_s\left(k_{m_nl_n}r_L\right)}{\partial r_L}e^{-i\Lambda}\right]\right\} \tag{2.21}$$

where, $$\Lambda=\left(\omega_o-s\omega_c\right)\tau+\omega_o t_o-s\phi-\left(m_n-s\right)\theta_o \tag{2.22}$$

After doing a similar procedure for the transverse momentum p_t, it can be obtained as

$$\frac{dp_t}{dt}=-|e|\,\mathrm{Re}\left\{\sum_{n=1}^{N}\frac{C_{m_nl_n}}{\omega_o}\left[\omega_o A_n\left(z,t\right)+i\nu_z\frac{\partial}{\partial z}A_n\left(z,t\right)\right]\times\left[\left(-i\right)^{s-1}J_{m_n-s}\left(k_{m_nl_n}r_b\right)\frac{\partial J_s\left(k_{m_nl_n}r_L\right)}{\partial r_L}e^{-i\Lambda}\right]\right\} \tag{2.23}$$

$$\frac{d\Lambda}{dt}=\frac{s|e|}{p_t}\mathrm{Re}\left\{\sum_{n=1}^{N}\left[\begin{array}{l}\dfrac{C_{m_n l_n}}{\omega_o}i\left[\omega_o A_n(z,t)+iv_z\dfrac{\partial}{\partial z}A_n(z,t)-\dfrac{k_{m_n l_n}^2}{s\omega_c\gamma_o}A_n(z,t)\right]\times \\ (-i)^{s-1}J_{m_n-s}\left(k_{m_n l_n}r_b\right)\dfrac{s\partial J_s\left(k_{m_n l_n}r_L\right)}{\partial r_L}e^{-i\Lambda}\end{array}\right]\right\}+\omega_c\left(\frac{\omega_o}{\omega_c}-s\frac{\gamma_o}{\gamma}\right) \quad (2.24)$$

Therefore, one can finally obtain expressions for the momentum and phase of the particles [91] as,

$$\frac{dp_t}{d\bar{z}}=\frac{\gamma}{p_z}\sum_{n=1}^{N}f_n J_s'\left(\bar{k}_{nt}\bar{r}_L\right)\mathrm{Re}\left\{\left[h+i\frac{p_z}{\gamma\omega_o}\frac{dh}{d\bar{z}}\right]e^{-i}\left[\Lambda+\bar{\psi}_n\right]+(m_n-s)\Theta_o\right\} \quad (2.25)$$

$$\frac{d\Lambda}{d\bar{z}}=\bar{\omega}_o\left[1-\frac{s\bar{\omega}_c}{\bar{\omega}_o\gamma}\right]-\frac{s\gamma}{p_z p_t}\sum_{n=1}^{N}f_n\frac{J_s'\left(\bar{k}_{nt}\bar{r}_L\right)}{\bar{k}_{nt}\bar{r}_L}\mathrm{Re}\left\{\left[h+i\frac{p_z}{\gamma\bar{\omega}_o}\frac{dh}{d\bar{z}}-\frac{\bar{\omega}_{no}^2p_t^2}{s\bar{\omega}_c\bar{\omega}_o\gamma}h\right]e^{-i}\left[\Lambda+\bar{\psi}_n\right]+(m_n-s)\Theta_o\right\} \quad (2.26)$$

$$\frac{dp_z}{d\bar{z}}=\frac{p_t}{p_z\bar{\omega}_o}\sum_{n=1}^{N}f_n J_s'\left(\bar{k}_{nt}\bar{r}_L\right)\mathrm{Re}\left\{\left[i\frac{dh}{d\bar{z}}\right]e^{-i}\left[\Lambda+\bar{\psi}_n\right]+(m_n-s)\Theta_o\right\} \quad (2.27)$$

where, γ is given as $\gamma=\sqrt{1+p_t^2+p_z^2}$. The linearized mode phase parameter is given as,

$$\bar{\psi}_n(z)=\psi_n(t_o)+\left.\frac{d\psi_n}{dt}\right|_{t_o}z/v_z$$

where all the variables with bars are the normalized one which are given as,

$$\bar{r}_L=r_L/R_0,\ \bar{\omega}_c=\omega R_0/c,\ \bar{k}_{nt}=k_{nt}R_0,\ \bar{z}=z/R_0 \text{ and } \bar{\omega}_o=\frac{\omega_o R_0}{c}$$

After deriving the equation for the movement of electrons in the interaction structure using Lorentz's force equation, the equations for the evolution of the RF field to construct the source term in the governed wave equation is derived. For the TE mode, the wave equation governing the transverse electric field is given as,

$$\nabla^2E_t-\frac{1}{c^2}\frac{\partial^2E_t}{\partial t^2}=\mu_o\frac{\partial J_t}{\partial t} \quad (2.28)$$

where, J_t stands for transverse AC current density. The transverse electric field E_t in the complex form is given by

$$E_t=\sum_{n=1}^{N}A_n(z,t)e_n(r,\theta)e^{-i\omega_o t} \quad (2.29)$$

Combining the above two equations, comparing the slow temporal amplitude variation (envelopes) of the sinusoidal RF field with the frequency of oscillation ω_o, *i.e.*, $\frac{\partial A_n}{\partial t} \ll \omega_o A_n$, and integrating over the cavity cross-section, the expression for n[th] mode is as follows,

$$\left[\frac{\partial^2}{\partial z^2} + \frac{\omega_o^2 - \omega_{nc}^2}{c^2} + 2i\frac{\omega_o}{c^2}\frac{\partial}{\partial t}\right] A_n(z,t) = -i\mu_o\omega_o \iint dS e_n^* J_{\omega_o} \tag{2.30}$$

The current density is expressed as $J_t = J_\omega e^{-i\omega_o t}$, where, $J_\omega = \int_0^{2\pi} J_t e^{i\omega_o t} d(\omega_o t)$ is the infinitesimal area element of waveguide's cross-section perpendicular to its axis. Therefore,

$$\nabla^2 E_t = \left(\nabla_t^2 + \frac{\partial^2}{\partial z^2}\right) E_t = \left(-k_{nc}^2 + \frac{\partial^2}{\partial z^2}\right) E_t = \left(-\frac{\omega_{nc}^2}{c^2} E_t + \frac{\partial^2}{\partial z^2}\right) E_t$$

$$\frac{\partial^2}{\partial t^2}\left[A_n(z,t)e^{-i\omega_o t}\right] = \left[\frac{\partial^2}{\partial t^2} - 2i\omega_o\frac{\partial}{\partial t} - \omega_o^2\right] A_n(z,t)e^{-i\omega_o t}$$

Using an orthogonal property of the vector functions as follows,

$$\iint e_{m_n l_n} . e^*_{p_n q_n} dS = \delta_{m_n l_n . p_n q_n}$$

$$\delta_{m_n l_n . p_n q_n} = 1, \quad \mathrm{m}_n = p_n \text{ and } \mathrm{l}_n = q_n$$
$$\delta_{m_n l_n . p_n q_n} = 0, \text{ otherwise}$$

To obtain the slow-time-scale equations for a gyrotron oscillator, multiply (2.30) by A_n^* and the complex conjugate of (2.30) by A_n. These two resulting equations are added and subtracted and then integrated into these sums or difference at the cavity's axial extent. The difference leads to

$$\begin{aligned} &\int_0^L \left[A_n^* \frac{\partial^2}{\partial z^2} A_n - A_n \frac{\partial^2}{\partial z^2} A_n^* + 2i\frac{\omega_o}{c^2}\left[A_n^*\frac{\partial}{\partial t}A_n + A_n\frac{\partial}{\partial t}A_n^*\right]\right] dz = -i\mu_o\omega_o \iiint \left[A_n^* e_n^* J_{\omega_o} + A_n e_n J_{\omega_o}^*\right] dS dz \\ &\Rightarrow \int_0^L \left[A_n^* \frac{\partial^2}{\partial z^2} A_n - A_n \frac{\partial^2}{\partial z^2} A_n^* + 2i\frac{\omega_o}{c^2}|A_n|^2\right] dz = -i\mu_o\omega_o \iiint \left[A_n^* e_n^* J_{\omega_o} + A_n e_n J_{\omega_o}^*\right] dS dz \end{aligned} \tag{2.31}$$

Similarly, the summation leads to

$$\int_0^L \left[A_n^* \frac{\partial^2}{\partial z^2} A_n + A_n \frac{\partial^2}{\partial z^2} A_n^* + 2\frac{\omega_o^2 - \omega_{nc}^2}{c^2} A_n A_n^* + 2i\left[A_n^* \frac{\partial}{\partial t} A_n - A_n \frac{\partial}{\partial t} A_n^* \right] \right] dz = -i\mu_o \omega_o \iiint \left[A_n^* e_n^* J_{\omega_o} - A_n e_n J_{\omega_o}^* \right] dS dz \qquad (2.32)$$

Integrating $\int_0^L \left[A_n^* \frac{\partial^2}{\partial z^2} A_n + A_n \frac{\partial^2}{\partial z^2} A_n^* \right] dz$ by parts, one can be obtained

$$\left(A_n^* \frac{\partial}{\partial z} A_n - A_n \frac{\partial}{\partial z} A_n^* \right) \Bigg|_0^L \qquad (2.33)$$

In the same way, integrating $\int_0^L \left[A_n^* \frac{\partial^2}{\partial z^2} A_n + A_n \frac{\partial^2}{\partial z^2} A_n^* \right] dz$, one can be obtained $\left(\frac{\partial}{\partial z} |A_n|^2 \right) \Bigg|_0^L - 2\int_0^L \left| \frac{\partial}{\partial z} A_n \right|^2$. By considering only an outgoing wave at $z = L$, *i.e.*, $A_n(z = L, t) = a_{nL}(t) \exp i\left[k_{nz} z - \psi_n(t) \right]$, it can be expressed as

$$A_n^* \frac{\partial}{\partial z} A_n - A_n \frac{\partial}{\partial z} A_n^* \Bigg|_0^L = 2ik_{nz} a_{nL}^2(t).$$

The following steps are followed to obtain the above relation. The separable form approximates $a_n(z, t)$ inside the cavity

$$A_n(z,t) = a_n(t) e^{i\left[-\psi_n(t)\right]} h_n(z) \qquad (2.34)$$

where $h_n(z)$ is the cavity field profile function which satisfies the Helmholtz equation

$$\left[\frac{d^2}{dz^2} + k_{nz}^2 \right] h_n(z) = 0 \qquad (2.35)$$

In this formulation, the beam loading effect on cavity field profile $h_n(z)$ is neglected. The possible choice for the field profile $h_n(z)$ is the Gaussian profile and sinusoidal profile. The Gaussian profile is used for the axial index number q =1. The Gaussian profile $h_n(z) = \exp\left[-(k_{nz} z)^2 \right]$ is centered at the cavity midpoint, where $k_{nz} = 2 / L$ is the effective axial wave number and L is the cavity's length. The sinusoidal profile is used for axial index numbers, q $\geq$ 2. The sinusoidal profile is given as $h_n(z) = \sin(k_{nz} z)$,

where, $k_{nz} = q\pi / L$ and 'q' is the axial index number.

The mode amplitude output in the cavity can be related to the mode amplitude in the cavity output through the Q-factor. According to this, the $a_{nL}(t)$, an (t) and quality factor (Q_n) are related as,

$$a_{nL}(t) = \left[\frac{W}{k_{nz}Q_n}\right]^{1/2} \frac{\omega_o}{c} a_n(t) \tag{2.36}$$

$$Q = \frac{\omega_o}{P_{out}} W_{energy} \tag{2.37}$$

where, $W_{energy} = \frac{1}{2}\varepsilon_o \int_0^L \left|A_n(z,t)\right|^2 dz$, therefore

$$P_{out} = \frac{1}{2\mu_o\varepsilon_o} k_{nz} \left|A_n(z=L,t)\right|^2 = \frac{1}{2\mu_o\varepsilon_o} k_{nz} a_{nL}^2(t) \tag{2.38}$$

$$Q_n = \frac{\omega_o \frac{1}{2}\varepsilon_o a_n^2(t).W}{\frac{1}{2\mu_o\varepsilon_o} k_{nz} a_{nL}^2(t)} \tag{2.39}$$

By using (2.36), (2.33) can be expressed as,

$$\left(A_n^* \frac{\partial}{\partial z} A_n - A_n \frac{\partial}{\partial z} A_n^*\right)\Big|_0^L = 2ik_{nz} a_{nL}^2(t) = 2ik_{nz} \frac{W}{k_{nz}Q_n} \frac{\omega_o^2}{c^2} a_n^2(t) \tag{2.40}$$

And the difference equation (2.31) can be expressed as,

$$\begin{aligned} \int_0^L \left[A_n^* \frac{\partial^2}{\partial z^2} A_n - A_n \frac{\partial^2}{\partial z^2} A_n^* + 2i\frac{\omega_o}{c^2}\left|A_n\right|^2\right] dz &= 2ik_{nz} \frac{W}{k_{nz}Q_n} \frac{\omega_o^2}{c^2} a_n^2(t) + 2iW \frac{\omega_o}{c^2} \frac{d}{dt} a_n^2(t) \\ &= -i\mu_o\omega_o \iiint \left[A_n^* e_n^* J_{\omega_o} + A_n e_n J_{\omega_o}^*\right] dSdz \end{aligned} \tag{2.41}$$

$$\frac{1}{Q_n}\frac{\omega_o^2}{c^2} a_n^2(t) + 4\frac{\omega_o}{c^2} a_n(t) \frac{d}{dt} a_n(t) = -\mu_o\omega_o a_n(t).\mathrm{Im}\left[\frac{i}{W} \iiint \left[h_n(z) e_n^* J_{\omega_o} \exp i\left[\psi_n(t)\right]\right] dsdz\right] \tag{2.42}$$

Thus the differential equation governing the mode amplitude and phase is obtained as,

$$\frac{d}{dt} a_n(t) + \frac{\omega_o}{2Q_n} a_n(t) = -\frac{1}{2\varepsilon_o}.\mathrm{Im}\left[\frac{i}{W} \iiint \left[h_n(z) e_n^* J_{\omega_o} \exp i\left[\psi_n(t)\right]\right] dsdz\right] \tag{2.43}$$

$$\frac{d}{dt}\psi_n(t)+\omega_o=\omega_{nc}-\frac{1}{2\varepsilon_o a_n(t)}\mathrm{Re}\left[\frac{i}{W}\iiint\left[h_n(z)e_n^* J_{\omega_o}\exp i\left[\psi_n(t)\right]\right]dSdz\right] \quad (2.44)$$

After substituting below modifications (Eqn. 2.45 & 2.46) and assumptions (h_n as symmetrical) in the summation equation (2.32)

$$\left[A_n^*\frac{\partial}{\partial t}A_n-A_n\frac{\partial}{\partial t}A_n^*\right]=-2ih_n^2(z)a_n^2(t)\frac{d}{dt}\psi_n(t) \quad (2.45)$$

$$\int_0^L\left|\frac{\partial}{\partial z}A_n\right|^2dz=a_n^2(t)\int_0^L\left|\frac{dh_n}{dz}\right|^2dz=0 \quad (2.46)$$

And h_n is assumed to be symmetrical, as in this case now, $\left(\frac{\partial}{\partial z}|A_n|^2\right)\Big|_0^L=0,$ since $A_n\to 0$ at the input cavity and A_n = constant at the cavity output. Hence,

$$\begin{aligned}&\int_0^L\left[2\frac{\omega_o^2-\omega_{nc}^2}{c^2}a_n^2(t)h_n^2(z)+4\frac{\omega_o}{c^2}\left[a_n^2(t)h_n^2(z)\frac{d}{dt}\psi_n(t)\right]\right]dz\\&=-2\mu_o\omega_o a_n(t)\mathrm{Re}\left[i\iiint\left[h_n(z)e_n^*J_{\omega_o}\exp\left[i\{\psi_n(t)\}\right]\right]dsdz\right]\end{aligned} \quad (2.47)$$

Approximating, $\omega_o^2-\omega_{nc}^2$ as $2\omega_o(\omega_o-\omega_{nc}),$ it is obtained as,

$$\begin{aligned}&\left[4\frac{\omega_o(\omega_o-\omega_{nc})}{c^2}a_n^2(t)h_n^2(z)+4\frac{\omega_o}{c^2}\left[a_n^2(t)h_n^2(z)\frac{d}{dt}\psi_n(t)\right]\right]\int_0^L h_n^2(z)dz=\\&=-2\mu_o\omega_o a_n(t)\mathrm{Re}\left[\mathrm{i}\iiint\left[h_n(z)e_n^*J_{\omega_o}\exp\left[i\{\psi_n(t)\}\right]dsdz\right]\right]\end{aligned} \quad (2.48)$$

$$\begin{aligned}&\left[4\frac{\omega_o(\omega_o-\omega_{nc})}{c^2}a_n^2(t)h_n^2(z)+4\frac{\omega_o}{c^2}\left[a_n^2(t)h_n^2(z)\frac{d}{dt}\psi_n(t)\right]\right]\\&=-2\mu_o\omega_o a_n(t)\mathrm{Re}\left[\frac{i}{\int_0^L h_n^2(z)dz}\right]\iiint\left[h_n(z)e_n^*J_{\omega_o}\exp\left[i\{\psi_n(t)\}\right]dsdz\right]\end{aligned} \quad (2.49)$$

With the help of these equations, the normalized RF field amplitude and phase of the mode can be obtained from (2.43) and (2.44) as [74],

$$\frac{df_n}{d\tau}=-\frac{f_n}{2Q_n}+\bar{I}_n\int_0^L d\bar{z}h(\bar{z})\left\langle J_s'(k_{nt}\bar{r}_L)\frac{p_t}{p_z}\cos\left[\left[\Lambda+\bar{\psi}_n\right]+(m_n-s)\Theta_o\right]\right\rangle_{\Lambda_o,\Theta_o} \quad (2.50)$$

$$\frac{d\Psi_n}{d\tau} = -\frac{\omega_o - \omega_{no}}{2Q_n} - \frac{\bar{I}_n}{f_n}\int_0^L d\bar{z}\,h(\bar{z})\left\langle J_s'(k_{nt}\bar{r}_L)\frac{p_t}{p_z}\sin\left[\left[\Lambda + \bar{\psi}_n\right] + (m_n - s)\Theta_o\right]\right\rangle_{\Lambda_o,\Theta_o} \tag{2.51}$$

where, $f_n = \frac{|e|}{m_e c^2}\chi_n' C_n J_{m_n-s}^2(k_{nt} r_b) a_n(t_o)$, and normalized current I_n is given by

$$I_n = \frac{|e| Z_o}{m_e c^2 \bar{\omega}_o}\frac{J_{m_n-s}^2(k_{nt}R_b)}{\pi\left(1 - \frac{m_n^2}{\chi_{m_n l_n}^2}\right)J_{m_n}^2(\chi_{m_n l_n}^2)\bar{W}} I_o \tag{2.52}$$

In the above equation (2.52), for co-rotating modes, m_n is considered to be greater than zero ($m_n > 0$) and for counter-rotating modes, $m_n < 0$. Therefore, the final expression for the time-dependent output power is obtained as,

$$P_n(\tau) = \frac{\pi m_o c^4}{2Z_o|e|^2}\frac{\left(1 - \frac{m_n^2}{\chi_{m_n l_n}^2}\right)J_{m_n}^2(\chi_{m_n l_n})}{J_{m_n-s}^2(k_{nt}R_o)}\bar{\omega}_o\bar{W}\left|f_n(\tau)\right|^2, \tag{2.53}$$

And the total efficiency can be obtained by the energy distribution of all particles as,

$$\eta = \frac{\gamma_o\left\langle\gamma(z=L)\right\rangle_{\Delta_o\Theta_o}}{\gamma_o - 1} \tag{2.54}$$

where $\langle\ \rangle_{\Delta_o\Theta_o}$ denotes the average over all the initial phase of all the particles.

2.3 Design Methodology and Limiting Constraints

The RF interaction structure is an important part of the gyrotron sub-assembly, in which beam-wave interaction taking place. To achieve the stable operation of the gyrotron, it is necessary not only to properly design the RF structure but also to have the selection of judicious beam parameters. To achieve the optimum performance of a gyrotron, it is required to optimize both electrical and structural parameters. These parameters should be selected according to the design constraints [1], [86]. Design approaches and design constraints are discussed in detail in further sections.

2.3.1 Mode Selection

For the stable operation of gyrotron, it must be operated at a constant frequency to generate a constant power. This is possible only when gyrotron is operated in a single mode. In parasitic mode, the device operation reduces the efficiency of device and also changes its resonant frequency. Although the operation in a higher-order mode is beneficial in terms of breakdown and power handling, this brings mode competition. The operating mode is chosen in such a way that has sufficient frequency separation from its nearby modes. Mode selection in the gyrotron is often achieved by magnetic field selection and/or proper selection of the beam radius. The starting current of the parasitic modes is greater than the operating current. Therefore, the gyrotron's appropriate design ensures that the operation in the desired mode is better than the operation in the parasitic modes.

For the $TE_{m,n}$ mode, the wall radius (r_W) of the gyrotron cavity is given by

$$R_o = \frac{\chi_{mn} c}{2\pi f} \tag{2.55}$$

where 'f' is the operating frequency, 'c' is the velocity of light and χ_{mn} is the nth root of the derivative of Bessel's function $J'_m(x) = 0$. The optimum beam radius (R_b) is given by

$$R_b = \frac{\chi_{m\pm s} R_o}{\chi_{mn}} = \frac{\chi_{m\pm s} c}{2\pi f} \tag{2.56}$$

where 's' is the harmonic number. Generally, '+' sign chosen for counter-rotating and '–' sign chose for co-rotating mode, which provides better coupling of the electron beam to the RF wave [1].

2.3.2 Cavity Losses

There are two main types of losses present in the gyrotron structure: ohmic loss (wall loss) and diffractive loss. The ohmic loss (wall loss) is a major problem, making it

impossible for the device to operate in long pulses or CW due to the wall losses. Power deposited in the cavity walls as ohmic loss represented as P_{ohm} and power lost by diffraction represented as output power P_{out}. Therefore, the total power lost in the cavity is $P_T = P_{ohm} + P_{out}$, which is related to the cavity quality factor Q at a cavity resonant frequency ω as,

$$Q = \frac{\omega U}{P_T} = \frac{\omega U}{dU/dt} \tag{2.57}$$

where, U is the stored energy in the resonator (cavity) volume V. The stored energy U in the resonator is given by

$$U = \frac{\varepsilon_o}{2}\int_V |E|^2 \, dV = E_o^2 \varepsilon_o \frac{\pi}{2k_{mn}^2}\left(\chi_{mn}^2 - m^2\right) J_m^2\left(\chi'_{mn}\right) \int_0^L \left|f(z)\right|^2 dz \tag{2.58}$$

For a Gaussian profile function $f(z) = \exp\left(-4z^2/L^2\right)$, the stored energy U can be represented as,

$$U = \varepsilon_o E_o^2 \left(\frac{\pi}{2}\right)^{3/2} \frac{L}{2k_{mn}^2}\left(\chi_{mn}^2 - m^2\right) J_m^2\left(\chi_{mn}\right) \tag{2.59}$$

The ohmic loss is related to its ohmic Q-factor as, $Q_{ohm} = \omega U / P_{ohm}$ and the diffractive loss is related to its diffractive Q-factor as, $Q_D = \omega U / P_{out}$, then the resonator Q-factor (Q_T) can be represented as,

$$\frac{1}{Q_T} = \frac{1}{Q_{ohm}} + \frac{1}{Q_D} \tag{2.60}$$

where, P_{ohm} is the wall loss and P_{out} is the output power. Therefore, the cavity loss can be related to the Q-factor as,

$$P_{ohm} Q_{ohm} = P_{out} Q_D \tag{2.61}$$

Due to the finite wall conductivity (σ) of the gyrotron cavity, the ohmic loss density on the cavity surface is given as,

$$\rho_{ohm} = \frac{1}{2\sigma\delta}\left|\hat{n}\times H\right|^2_{r=r_b} = \frac{1}{2\sigma\delta\mu_o^2}\left(1+\frac{m^2k_z^2}{k_{mn}^2R_b^2}\right)\frac{k_{mn}^2}{\omega^2}E_o^2J_m^2\left(k_{mn}R_b\right)\left|f\left(z\right)\right|^2 \quad (2.62)$$

where, δ is the skin depth, σ is the electrical conductivity of the cavity wall. The bracket's second term is negligible in the cut-off limit, $k_z << k_{mn}$, where, k_z and k_{mn} are the axial and transverse wavenumbers, respectively. The expression of ohmic loss density can be expressed in terms of the normalized parameters, F, μ, and Δ as [86]

$$\rho_{ohm}\left(W/m^2\right) = 5.1\times10^{-15}\sigma^{-0.5}\omega^{2.5}F^2\beta_t^6C_t^2\gamma^2\left(1-0.5\beta_t^2\Delta\right)^2 \quad (2.63)$$

where, $C_t = J_m\left(k_{mn}\right)/J_{m\pm s}\left(k_{mn}R_b\right)$. This will provide the choice of the cathode voltage and field amplitude for a tolerable wall loss. The skin depth (δ) is given as,

$$\delta = \sqrt{\frac{2}{\omega\mu_o\sigma}} \quad (2.64)$$

By using (2.59), (2.62) and (2.64) in the expression of Q_{ohm} (2.61) under the gyrotron operating condition $k_z \ll k_{mn}$, the expression for Q_{ohm} is given as,

$$Q_{ohm} = \frac{r_c}{\delta}\left(1-\frac{m^2}{\chi_{mn}^2}\right) \quad (2.65)$$

The diffractive Q-factor of the gyrotron cavity is depending upon the cavity decay time and reflections at both ends of the cavity [1], [80]. The diffractive Q_D is given as,

$$Q_D = \frac{4\pi}{1-R_1R_2}\left(\frac{L}{\lambda}\right)^2 \quad (2.66)$$

where, L is the effective length of the cavity. By using (2.58), (2.61) and (2.62), the maximum wall loading can be estimated as,

$$\left(\frac{dP}{dA}\right)_{\max} \approx \frac{2\pi\delta}{\lambda^2}\frac{P_{out}Q_D}{\left(\chi_{mn}^2-m^2\right)L} \quad (2.67)$$

2.3.3 Voltage depression and limiting current

The voltage depression is one of the major limiting factors in the design of

gyrotrons [1], [98] – [99]. The voltage depression in the gyrotron operation affects its resonant frequency, velocity ratio (α), and velocity spread, which play a key role in reducing the gyrotron's efficiency. In a cylindrical cavity with the radius R_o, the potential depression V_{dep} between the cavity wall and the axis of symmetry due to a concentric electron beam with a uniform current density is given by [1], [98],

$$V_{dep} = \frac{1}{4\pi\varepsilon_o c}\frac{I_b}{\beta_z} G\left(r_i, R_b, r_o\right) \tag{2.68}$$

where, G is the geometrical factor is given as,

$$G\left(r_i, R_b, r_o\right) = 2\ln\left(\frac{R_o}{r_o}\right) + \left[1 - \frac{2r_i^2}{\left(r_o - r_i\right)^2}\ln\left(\frac{r_o}{r_i}\right)\right] \tag{2.69}$$

where, r_i and r_o are the inner and outer beam radii, respectively. The first term in (2.69) corresponds to a potential drop between the wall and the outer beam radius. The second term in (2.69) is responsible for the potential drop on the beam's thickness. For a thin annular electron beam $\left(R_b \approx r_o\right)$ and considering the guiding radius is for greater than the beam thickness $\left(R_b \gg r_o - r_i\right)$, the second term in (2.69) is approximated to 1. Hence, the geometrical factor (G) can be written as,

$$G\left(r_i, R_b, r_o\right) \approx 2\ln\left(\frac{R_o}{r_o}\right) \tag{2.70}$$

Therefore, the voltage depression from (2.68) can be written as,

$$V_{dep} \approx 60\frac{I_b}{\beta_z}\ln\left(\frac{R_o}{R_b}\right) \tag{2.71}$$

For a given momentum and cathode voltage, the limiting current can be determined due to the present potential depression. If the current is increased beyond I_L, the potential depression increases in such a way that the axial velocity of electrons becomes zero, therefore the beam is not propagated and is reflected back instead [1]. The relativistic

mass factor is also changes due to potential depression and is given by,

$$\gamma = 1 + \frac{e\left(V_b - V_{dep}\right)}{m_e c^2} \tag{2.72}$$

By using (2.68) and (2.72), the beam current can be expressed as,

$$I_b = 4\pi\varepsilon_o c \frac{\beta_z}{G}\left(V_b - \frac{m_e c^2}{e}\left(1-\beta_z^2-\beta_t^2\right)^{-1/2} - 1\right) \tag{2.73}$$

The limiting current I_L is obtained by maximizing the beam current (I_b) with respect to the axial velocity, while keeping the transverse momentum as constant.

$$\left.\frac{\partial I_b}{\partial \beta_z}\right|_{\gamma\beta_t = const} = 0 \tag{2.74}$$

By solving the (2.73) and (2.74), one can obtain the maximum value of the beam current I_b. The expression for the limiting current can be written as,

$$\begin{aligned} I_L(A) &= \frac{4\pi\varepsilon_o m_e c^3}{e}\gamma_o\left[1-\left(1-\beta_{zo}^2\right)^{1/3}\right]^{3/2}\frac{1}{G\left(r_i, R_b, r_o\right)} \\ &= 1.707\times10^4\gamma_o\left[1-\left(1-\beta_{zo}^2\right)^{1/3}\right]^{3/2}\frac{1}{G\left(r_i, R_b, r_o\right)} \end{aligned} \tag{2.74}$$

where, γ_o and β_o represent values in the absence of voltage depression. Using (2.70), for a thin electron beam the limiting current is given as,

$$\frac{I_L}{8500} \approx I^* \Big/ \ln\frac{R_o}{R_b} \tag{2.75}$$

where, $I^* = \gamma_o\left[1-\left(1-\beta_{zo}^2\right)^{1/3}\right]^{3/2}$.

2.3.4 Start oscillation current

For the device operation in the desired mode, a start-up scenario is investigated that needs to satisfy the conditions of self-excitation. This gives the nominal operating point, which ensures the desired mode excitation with the maximum efficiency at the desired output power, while suppressing the neighbouring modes. The self-excitation of

a gyrotron is characterized by a start oscillation current (I_{sc}) that depends on the beam parameters (such as beam voltage, beam current, beam radius, velocity ratio, etc.) and the magnetic field. As the beam current is slightly ahead of I_{SC} for a particular mode, the self-excitation condition is met and this mode starts oscillating in the gyrotron cavity. As long as the beam current does not exceed the threshold value of the start oscillation current, the gyrotron will not initiate the oscillation that depends on beam parameters, magnetic field, and resonator geometry. The start oscillation current of all nearby modes is calculated to ensure that the gyrotron is operated in the desired mode with optimum efficiency. The start oscillation current is calculated by the linear theory [85], [87], [99] – [101]. Analytically, the start oscillation current is the minimum current at which the rate of change of output power $dP_{out}/dt > 0$ in the limit $P_{out} \to 0$ [1]. The start oscillation current, I_{sc} can be given as,

$$I_{sc}V_b = \left(\left. \frac{d\eta}{dP_{out}} \right|_{P=0} \right)^{-1} \tag{2.76}$$

V_b is the accelerating voltage, η is the gyrotron's efficiency, and P_{out} is the output power. For the stable operation, $I_b > I_{sc}$ and $dP_{out}/dt > 0,$ otherwise oscillation will not start. The average over initial gyro-phase is now trivial and is observed as,

$$QP_{out} = Q\eta I_b V_b = \frac{1}{2}\omega\varepsilon_o \int_0^L \left| f_{mn}(z) \right|^2 dz = \frac{1}{2}\omega\varepsilon_o \int_0^L \left| \hat{f}(z) \right|^2 dz . \left\{ \frac{2m_e c^2}{e} \frac{\nu_{z_o}}{c\chi_{mn} C_{mn} G_{mn}} \right\}^2 \tag{2.77}$$

where, η is the efficiency and I_b is the beam current, $\chi_{mn}^2 C_{mn}^2 G_{mn}^2$ is the beam-field coupling factor of the electron beam to the RF wave. Using (2.77), (2.76) can be re-written as,

$$\frac{d\eta}{dP_{out}} = \frac{d\eta}{dF^2} \frac{1}{2} \frac{Q}{\omega\varepsilon_o} \left[\left(\frac{e}{m_e c^2} \right) \frac{\chi_{mn} C_{mn} G_{mn}}{\beta_{zo}} \right]^2 \frac{1}{\int \left| \hat{f}(z) \right|^2 dz} \tag{2.78}$$

By using (2.78), the expression for the start oscillation current for an arbitrary cyclotron

harmonic is given as,

$$\frac{-1}{I_{sc}}=\left(\frac{QZ_o e}{8\gamma_o m_e c^2}\right)\left(\frac{\pi}{\lambda}\int_0^L\left|\hat{f}(z)\right|^2 dz\right)^{-1}\left(\frac{\chi_{mn}C_{mn}G_{mn}}{\beta_{zo}(s-1)!}\right)^2\left(\frac{ck_{mn}\gamma_o\beta_{to}}{2\gamma_o}\right)^{2(s-1)}$$
$$\times\left(s+\frac{1}{2}\frac{\omega\beta_{zo}^2}{\nu_{zo}}\frac{\partial}{\partial\Delta_1}\right)\left|\int_0^L\hat{f}(z)\exp(j\Delta_1 zdz)\right|^2 \tag{2.79}$$

The Gaussian field profile shows the close approximation of the open cavities' field profile in the gyrotron [92].

$\hat{f}(z)=\exp\left[-\left(\frac{2z}{L}-1\right)^2\right]$, where, L is the length of the straight section of the cavity.

Therefore, from (2.79) we can obtain,

$$\left|\int_0^L\hat{f}(z)\exp(j\Delta_1 zdz)\right|^2\cong\frac{L^2\pi}{4}\exp\left[-\frac{(\Delta_1 L)^2}{8}\right] \tag{2.80}$$

The coupling coefficient for the TE mode between the electron beam RF waves is given as

$$C_o^{\pm}=\chi_{m,n}^2 C_{m,n}^2 J_{m\mp s}^2\left(\chi_{mn}\bar{R}_b\right)=\frac{\chi_{m,n}^2 J_{m\mp s}^2\left(k_{mn}\bar{R}_b\right)}{\left(\chi_{mn}^2-m^2\right)J_m^2(\chi_{mn})} \tag{2.81}$$

where, '+' sign of $C_o^{\pm}$ stands for the co-rotating mode and '–' sign of $C_o^{\pm}$ stands for counter-rotating mode. Using the expression of coupling coefficients, the optimal radius of the electron beam can be determined for the mode chosen for maximum coupling. Therefore, for Gaussian profiles the initial current in terms of μ and Δ is given as,

$$I_{start}(\Delta,\mu)=8.56\times10^4\frac{\exp\left[\frac{1}{8}(\mu\Delta)^2\right]}{\mu^2\left(\mu^2\Delta-4s\right)}\left(\frac{\gamma_o}{Q}\right)\beta_{t_o}^{2(3-s)}\left(\frac{L}{\lambda}\right)C_o^{-1} \tag{2.82}$$

where, μ is the normalized interaction length and Δ is the mode detuning parameter, which are given as,

$$\mu = \pi \frac{\beta_{to}^2}{\beta_{zo}} \frac{L}{\lambda} \tag{2.83}$$

$$\Delta = \frac{2}{\beta_{to}^2}\left(1 - \frac{s\omega_{co}}{\omega}\right) \tag{2.84}$$

For, sinusoidal profile, the start oscillation current is given as [102],

$$I_{start} = \frac{4\gamma\varepsilon_o m_e}{e}\frac{\omega}{Q}|p_o|^2 \frac{k_z^2 v_z^2}{C_{mn}^2} \times \left[s\beta_{to}^2 \frac{dF_c}{dz} - 2F_c \right]^{-1} \tag{2.85}$$

where,

$$|p_o|^2 = \frac{\pi L}{2}\frac{1}{k_{mn}^2}, \quad k_z = \frac{q\pi}{L}, \quad F_c = \frac{2}{\left(1-x^2\right)^2}\sin^2\left[\frac{(x+1)q\pi}{2}\right], x = \frac{\omega_c/\gamma - \omega}{k_z v_z}, \qquad \text{s=}\frac{\omega_c/\gamma}{k_z v_z}$$

It is noticed that the start oscillation current I_{sc} is inversely proportional to the square of the coupling coefficient, i.e. $I_{sc} \propto C_o^{-1}$. For a given mode with the small value of $C_o^{\pm}$, the value of the start oscillation current I_{sc} is high so that the mode is unlikely to oscillate for a small value of the beam current. Therefore, the electron beam must be positioned in such a way that to allow the maximum coupling between the electron beam and the RF wave for the desired mode. Equation (2.82) is used to calculate the start oscillation current for an arbitrary cyclotron harmonic mode with an axial mode number, q = 1 (Gaussian-like profile). For higher-order axial mode numbers ($q \geq 2$), equation (2.85) can be used to calculate the starting oscillation current. To achieve the desired output power at the desired frequency, the choice of operating mode, beam parameters, and the optimized geometry of the cavity is generally determined by a series of trade-offs involving with various performance-limiting constraints like ohmic losses in the cavity walls and mode competition in the cavity [1].

Table 2.1: Structural and Electrical Parameters of the Gyrotron [64], [65]

Structural Parameters	Down Taper	Length (mm)	10
		Angle	3^o
	Straight Section	Length (mm)	22
		Cavity Radius (mm)	2.369
	Up Taper 1 (UT 1)	Length (mm)	10
		Angle	1^o
	Up Taper 2 (UT 2)	Length (mm)	63
		Angle	2.24^o
Electrical Parameters	Voltage	15.5 kV	
	Current	0.1 A	
	Frequency	260.46 GHz	
	Pitch factor	≤ 2 (1 – 2)	
	Magnetic field	9.51 T – 9.71 T	
	Beam width	~0.066 mm	
	Beam radius	1.374 mm	
	Velocity spread	~2%	
	Output power	$\geq$ 1.5 W	

2.4 Results and Discussion

The gyrotron's design and analytical studies have been done with the developed Multimode code to examine its beam-wave interaction behavior. In the Multimode analysis, Runge – Kutta method is used to solve the differential equations. This code provides a comprehensive picture of the Multimode effect on the device's performance for arbitrary harmonic operation. The small initial amplitude is assigned to start the numerical integration and equal phase of the number off particles considered. In the present Multimode simulation, 64 macro-electrons or particles are considered in order to achieve the desired accuracy with a time step of 2 ps. All the electrons are assigned the initial transverse and longitudinal energy-based calculated from the beam voltage (V_b) and velocity pitch factor (α). The electrons are uniformly distributed over the interval [0, 2π] for the zero velocity spread. All the parameters like beam radius, beam

voltage, beam current, velocity ratio, velocity spread, and magnetic field are judiciously used in the Multimode simulation.

2.4.1 Design procedure of 260 GHz Gyrotron

To validate the developed design methodology and Multimode code, a 260 GHz CW gyrotron is considered, for which the design parameters are well established.

2.4.1.a RF Interaction Structure

The RF interaction cavity used in the present gyrotron is a three-segment structure consisting of a central smooth-walled cylindrical waveguide section and two linearly-tapered cylindrical waveguide sections, namely a down taper at the entrance and uptaper at the output. Both uptaper and down taper of the cavity provide the sufficient reflection to maintain a standing wave pattern in the straight section of the cavity. The down taper ensures the input section's cut-off condition, which prevents the backpropagation of RF wave towards the cathode region. Thebeam–wave interaction takes place mainly in the middle of the straight section of the cavity, where the RF field is usually maximum. The uptaper section of the cavity converts the standing wave into a traveling wave to couple the cavity energy to the output waveguide.

A conventional gyrotron cavity is modelled based on the experimentally tested gyrotron by Alberti *et al.* [64] – [65], operating in TE_{72}-mode at 260 GHz. The structural and electrical parameters of the 260 GHz cavity operating in $TE_{7,2}$ mode are given in the Table – 2.1.

2.4.1.b Cavity Field Profile

The RF field should be maximum at the mid of the cavity to achieve the maximum interaction. The calculation of the cavity field profile is based on a formulation given in [1], [103] – [105]. The cavity field profile of the cavity in the

absence of the electron beam is given by,

$$\frac{d^2 f\ z}{dz^2} = -\mathrm{k}^2 f\ z \tag{2.86}$$

with the boundary conditions at z = 0 and z = z_{out} are [88],

$$\left.\frac{df(z)}{dz}\right|_{z=0} = -ikf(z)$$
$$\left.\frac{df(z)}{dz}\right|_{z=z_{out}} = +ikf(z) \tag{2.87}$$

where, $f(z)$ is the RF field profile, $k = \sqrt{\omega^2/c^2 - \chi_{m,n}^2/R^2(z)}$ is the wave number, c is the velocity of light in free space, $R(z)$ is the radius along with axial direction and $\chi_{m,n}$ is the n^{th} root of the first derivative of Bessel function J_m, where, m and n are the azimuthal and radial indices, respectively. The complex frequency is $\omega = 2\pi f_0\ (1 + \mathrm{j}/2Q_d)$, where, f_o is the operating frequency, and Q_d is the diffractive quality factor. The normalized cavity field profile is calculated by using (2.86) and (2.87), as shown in Figure 2.1 that shows the normalized field as maximum in the middle of the straight section of the cavity, which is necessary for optimal beam-wave interactions in the cavity.

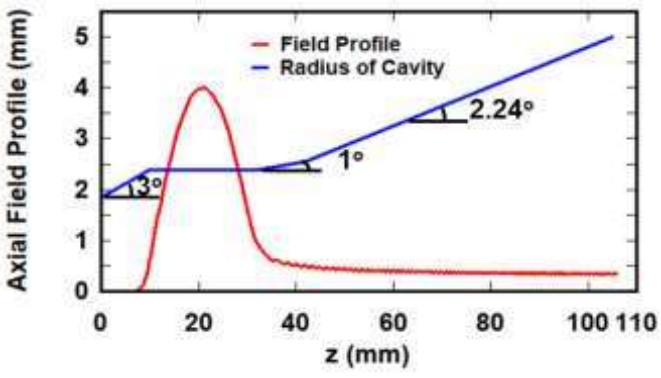

Figure 2.2 Radial profile and cavity field profile along the axial length of the cavity.

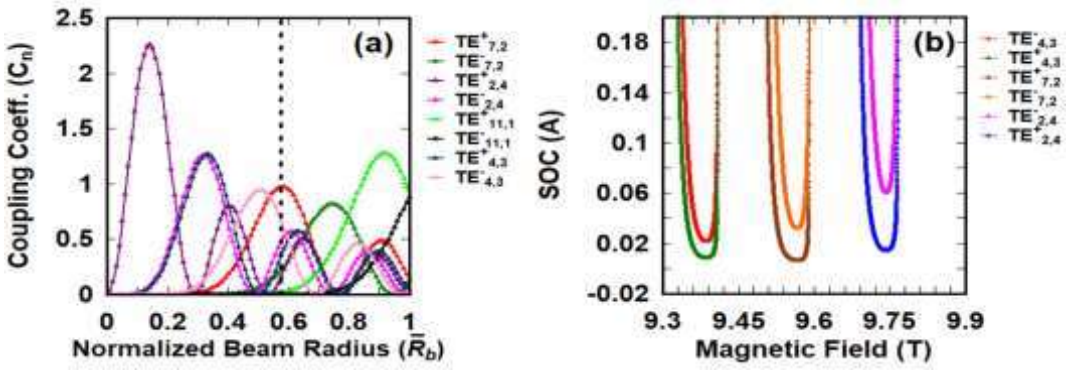

Figure 2.3 (a) Relation between the coupling coefficient and normalized beam radius, and (b) SOC of $TE_{7,2}$ mode and competing modes.

2.4.1.c Coupling Coefficient and Start Oscillation Current

The coupling coefficient between the electron beam and RF wave is calculated by using (2.81) in which '–' sign used for co-rotating mode and '+' sign used for counter-rotating mode. Using this, one can find the optimum beam radius to have maximum coupling for the chosen mode. In the present study, an RF cavity is operated in $TE^{+}_{7,2}$ mode at 260 GHz gyrotron. The operating mode is chosen as co-rotating one, as it has higher electron-wave coupling and lower start oscillation current (SOC). The coupling coefficient (C_n) of the co-rotating and counter-rotating modes of $TE_{7,2}$, $TE_{4,3}$, $TE_{11,1}$, and $TE_{2,4}$ are plotted as shown in Figure 2.3 (a). The coupling coefficient of the co-rotating $TE^{+}_{7,2}$ is found to be maximum at the normalized beam radius ~0.58, as compared to other nearby competing modes including a co-rotating $TE^{+}_{4,3}$, $TE^{+}_{2,4}$, $TE^{+}_{11,1}$ and the counter-rotating $TE^{-}_{4,3}$, $TE^{-}_{2,4}$, $TE^{-}_{11,1}$, $TE^{-}_{7,2}$ modes [Figure 2.3 (a)]. In other words, the coupling of the co-rotating $TE^{+}_{7,2}$ mode with the electron beam is found maximum at the electron beam radius (R_b) ~1.374 mm. The beam width is calculated as ~0.066 mm. The Figure 2.3 (a) shows that the $TE_{4,3}$ and $TE_{2,4}$ are the spurious competing modes. However, the $TE_{4,3}$ and $TE_{2,4}$ modes have enough frequency

separation from the operating $TE_{7,2}$ mode. Therefore, these modes can be suppressed easily by choosing the proper magnetic field.

The start oscillation current (I_{sc}) is a minimum current at which gyrotron starts oscillation. A gyrotron will not oscillate if the current is below this threshold value I_{sc}, which depends on beam properties, magnetic field, resonator geometry, etc. A comparison of the starting oscillation current between the desired and competing modes determines whether the desired mode is excited with maximum efficiency at the desired power level while pushing the neighboring mode. The start oscillation current (SOC) [Figure 2.3 (b)] of the operating mode $TE_{7,2}^{+}$ and other competing modes is calculated using (2.82) on the design parameters given in Table – 2.1. The SOC of the operating $TE_{7,2}^{+}$ is found minimum at ~9.55 T.

2.4.2 Numerical Benchmarking

A time-dependent Multimode code has been developed to investigate the beam-wave interaction behavior of the gyrotron. The code has been benchmarked with the 260 GHz gyrotron results [64] – [65], in which the output power in operating mode $TE_{7,2}$ with the other competing modes like $TE_{2,4}$, $TE_{11,1}$, and $TE_{4,3}$ are examined. In the Multimode simulation, the electrical parameters are taken as mentioned in Table – 2.1. The output power is calculated as ~163 W in the operating $TE_{7,2}$ mode and negligible power in other competing modes ($TE_{2,4}$, $TE_{11,1}$, and $TE_{4,3}$) by using Multimode code. Alberti *et al.* [65] have obtained ~ 152 W powers in the experiment of 260 GHz gyrotron. The Multimode simulation results are observed to be in good agreement with experimental results by ~6%, as shown in Figure 2.4.

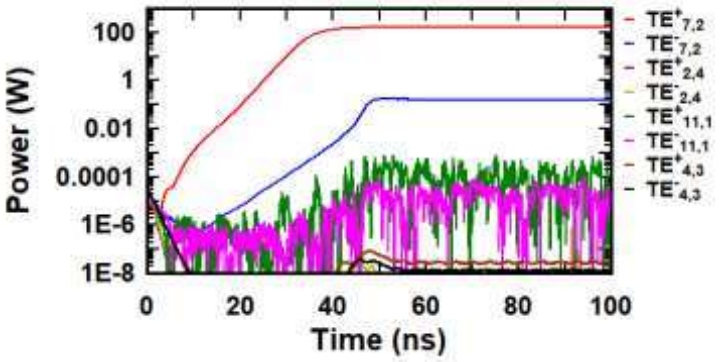

Figure 2.4 The output power of operating $TE_{7,2}$ mode and other competing modes using Multimode code (For beam parameters V_b = 15.5 keV, I_b = 0.1 A, B_o = 9.52 T and α = 1.12).

2.5 Conclusion

In the present chapter, an overview of existing analysis has been revisited and its application to design the gyrotron accordance with the various limiting constraints is discussed. Nonlinear analysis is used to investigate beam-wave interactions in the gyrotron cavity. The linear theory is used to predict start oscillation conditions that provide the basis for gyrotron design and its understanding. Nonlinear analysis is used to predict output power, efficiency, and bunching phenomena that understand the beam-wave interaction mechanism in the gyrotron. These gyrotron oscillator analyses are generalized and incorporate the device operation in arbitrary cyclotron harmonics employing any arbitrary shape of the interaction structures. The motion of the electron beam is represented by a couple of energy and phase equations, resulting in a simplification of the equations and also reducing their number.

In the gyrotron's practical design, various limiting constraints such as wall loss, voltage depression, and limiting current are played an important role, which is discussed in detail. These limited constraints are restricted the mode selection, electron beam parameters, and structural parameters because they affect the performance of the gyrotron. To observe the effect of these limiting constraints, the codes are developed

based on the described analysis. For the validity of these codes, they are benchmarked against existing published results. A systematic design procedure of the 260 GHz gyrotron is presented in which the cavity field profile, coupling coefficient, and start oscillation current are discussed. Some codes have been developed for calculating cavity field profiles, coupling coefficients, and start oscillation currents. The results obtained from these codes have been validated with experimental results.

A code based on nonlinear Multimode analysis has been developed to observe the output power and bunching mechanism. To benchmark, this developed code, the beam parameters in the Multimode simulation have been taken to be similar to the experimental 260 GHz gyrotron. The developed Multimode codes have seen good agreement for published experimental results with a difference of ~6 %. The present design methodology will be used in subsequent chapters in the design and analysis of the gyrotron.